


First-principles study on the electronic and magnetic properties of monolayer FeSe on Cu₃N(001)Hui-Hui He¹, Xiao-Le Qiu², Ben-Chao Gong³, Zhong-Yi Lu^{1,4,*} and Kai Liu^{1,4,†}¹*Department of Physics and Beijing Key Laboratory of Opto-electronic Functional Materials & Micro-nano Devices, Renmin University of China, Beijing 100872, China*²*School of Physics and Electronic Information, Weifang University, Weifang 261061, China*³*Department of Physics, School of Science, Jiangsu University of Science and Technology, Zhenjiang 212100, China*⁴*Key Laboratory of Quantum State Construction and Manipulation (Ministry of Education), Renmin University of China, Beijing 100872, China* (Received 10 June 2023; revised 6 September 2023; accepted 12 September 2023; published 25 September 2023)

The significantly enhanced superconductivity in the FeSe monolayer on oxide substrates like SrTiO₃(001), for which the electron doping from the substrate to the FeSe monolayer is considered a key factor, has attracted extensive interest in the past decade. Here, based on the first-principles electronic structure calculations, we propose that Cu₃N(001) is a promising hole-doping substrate for tuning the electronic and magnetic properties of the epitaxially grown FeSe monolayer. Due to the in-plane lattice strain and the electron redistribution at the FeSe/Cu₃N interface, strong magnetic frustration between the dimer and stripe antiferromagnetic states may exist in the FeSe monolayer. According to the charge transfer analysis, the Cu₃N substrate can dope ~ 0.02 hole per Fe atom to the FeSe monolayer, and the hole doping level can be partially modulated by the external electric field and/or the Cu vacancies in the substrate. These results indicate that FeSe/Cu₃N is a prospective platform for exploring the hole-doped superconductivity in the FeSe-based interfacial system, which may serve as a model system in contrast to electron-doped FeSe/SrTiO₃.

DOI: [10.1103/PhysRevB.108.115147](https://doi.org/10.1103/PhysRevB.108.115147)**I. INTRODUCTION**

FeSe has the simplest layered structure among the iron-based superconductors, and its physical properties can be effectively modulated via diverse approaches such as atom/molecule intercalation [1,2], chemical substitution [3], the application of pressure [4], and gating techniques [5]. As an example of one aspect, bulk FeSe shows a superconducting transition temperature $T_c \sim 9$ K at ambient conditions [6], while its superconducting T_c can largely be regulated through electron doping. Especially, $K_x\text{Fe}_{2-y}\text{Se}_2$, $(\text{TBA})_x\text{FeSe}$, and FeSe flakes under electrostatic doping show respective superconducting T_c as high as 31 K [7], 43 K [8], and 48 K [5], which are much higher than that of bulk FeSe. More astonishingly, monolayer FeSe epitaxially grown on a SrTiO₃ (STO) substrate demonstrates a superconducting gap even above 65 K [9–12]. As to the significantly enhanced superconductivity in FeSe/STO, it has been proposed that many effects may be relevant, including electron doping [13,14], interfacial phonons [15], lattice strain [16], polarons [17], and magnetism [18,19]. Compared with FeSe-derived bulk materials, the FeSe/STO interfacial system provides an ideal platform to directly tune and detect the quantum states in a single FeSe layer.

In order to comprehensively explore the interfacial superconductivity of the epitaxy FeSe monolayer, a variety

of substrates, such as SrTiO₃ [8,9,12,18,19], BaTiO₃ [16], TiO₂ [20,21], MgO [22], and LaFeO₃ [23], have been adopted. Those substrates are mainly the oxides, which inevitably introduce oxygen defects, so they tend to dope electrons to the FeSe epitaxial film. Similar to the oxides, many nitrides are also stable compounds with semiconducting and polarization features. For example, Cu₃N is a cubic nitride constructed by alternating Cu₂N and Cu layers with an in-plane lattice constant of 3.82 Å [24], which matches quite well with that of FeSe. Moreover, Cu₃N is a semiconductor with a band gap of about 1.5 eV [25] and exhibits bipolar doping behavior [26]. When Cu₃N grows on the Fe substrate [27], its surface is often Cu₂N terminated, which can induce surface charge accumulation and may serve as a hole dopant for epitaxial films such as FeSe.

In this paper, we investigate the electronic and magnetic properties of monolayer FeSe on the Cu₃N(001) surface by means of the first-principles calculations. We find that for monolayer FeSe at the optimal epitaxial position on Cu₃N(001), the dimer antiferromagnetic (AFM) state and the stripe AFM state are almost energetically degenerate, which implies the existence of strong magnetic frustration. In comparison with the electron doping in FeSe/STO, there are holes doped to the FeSe film from the Cu₃N substrate, which can be partially enhanced via the electric field and/or the Cu vacancies in Cu₃N. By examining the magnetism and the charge transfer in FeSe/Cu₃N, we propose that Cu₃N may be a promising substrate for realizing the hole-doped interfacial superconductivity of FeSe.

*zlu@ruc.edu.cn

†kliu@ruc.edu.cn

II. COMPUTATIONAL DETAILS

The first-principles calculations were performed based on the density functional theory (DFT) [28,29] and the projector augmented wave method [30,31] as implemented in the Vienna Ab initio Simulation Package (VASP) [32]. The generalized gradient approximation (GGA) of Perdew-Burke-Ernzerhof type [33] was utilized for the exchange-correlation functionals. The kinetic energy cutoff of the plane-wave basis set was set to 520 eV. The in-plane lattice constant of $a = 3.82 \text{ \AA}$ was taken from the experimental value of Cu_3N [24]. To model the Cu_3N substrate, we used a 10-layer slab with the bottom seven layers fixed at the bulk positions. A vacuum layer ($\sim 20 \text{ \AA}$) was employed to eliminate the artificial interaction between the image slabs along the z direction. The possible van der Waals interaction between the FeSe monolayer and Cu_3N substrate was described by the DFT-D2 method [34,35]. Γ -centered $8 \times 8 \times 1$ and $6 \times 4 \times 1$ Monkhorst-Pack [36] k -point meshes were used for the Brillouin zone samplings of the unit cell and the $\sqrt{2} \times 2 \sqrt{2}$ supercell, respectively. The Gaussian smearing method with a width of 0.05 eV was adopted for the Fermi surface broadening. The internal atomic positions were fully optimized until the forces on all unfixed atoms were smaller than 0.01 eV/\AA . We also performed calculations of the Fermi surfaces by using the VASPKIT code [37] and exhibited them via the FermiSurfer program [38]. The correlation effect among Cu $3d$ electrons was incorporated using the GGA+ U formalism of Dudarev *et al.* [39]. Following previous studies [40,41], we chose an effective Hubbard U of 5.0 eV on Cu $3d$ orbitals, which can describe the indirect band gap of Cu_3N as detected by x-ray diffraction and optical measurements of Cu_3N thin films [42]. We also found that a modest enhancement of Hubbard U in Cu $3d$ orbitals and the inclusion of Hubbard U in Fe $3d$ orbitals ($U = 0.5 \text{ eV}$ as in Ref. [43]) do not change our major conclusions on the electronic and magnetic properties of FeSe/ Cu_3N . When calculating the charge transfer, we used the structures of the FeSe layer and Cu_3N slab directly separated from the relaxed FeSe/ Cu_3N heterostructure. Then the transferred charge densities $\rho_{\text{trans}} = \rho(\text{FeSe}/\text{Cu}_3\text{N}) - \rho(\text{FeSe}) - \rho(\text{Cu}_3\text{N})$ were averaged in the ab plane and integrated along the c axis to get the charge transfer value. To simulate the doping effects of F and O in the Cu_3N substrate, we established a 10-layer $\sqrt{2} \times 2 \sqrt{2}$ Cu_3N slab and added a F or O atom in this slab to get 5% doped F or O. The upper three layers of these slabs were relaxed, and the work functions were obtained by determining the potential energy difference between the vacuum level and the Fermi level of the slab ($\text{WF} = E_{\text{vacuum}} - E_{\text{Fermi}}$).

III. RESULTS

Bulk Cu_3N has a cubic crystal structure (space group $Pm\bar{3}m$) with the Cu_2N and Cu layers stacking alternately along the $[001]$ direction (Fig. 1). By controlling the growth conditions, the surface termination of $\text{Cu}_3\text{N}(001)$ can be either the Cu_2N layer or the Cu layer [42]. According to a previous report, the $\text{Cu}_3\text{N}(001)$ surface is usually formed in a N-rich environment [44]; thus, we focus on only the Cu_2N -terminated $\text{Cu}_3\text{N}(001)$ surface in the following. We first

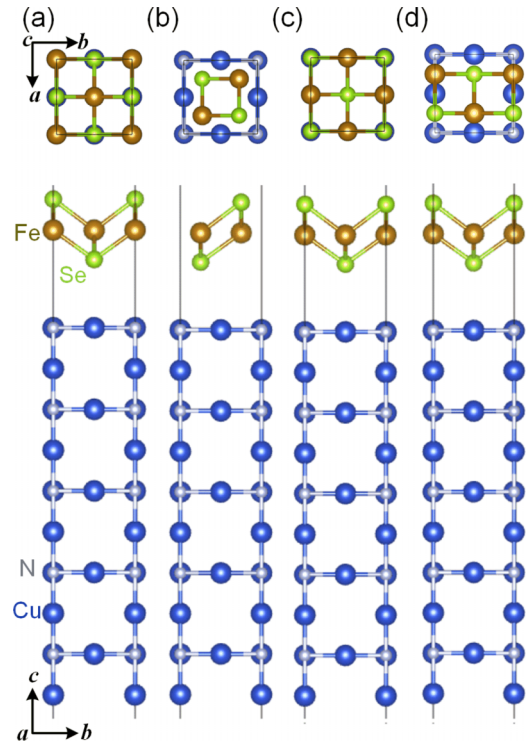


FIG. 1. Four possible epitaxial structures of FeSe/ $\text{Cu}_3\text{N}(001)$. The upper and lower parts of each panel show the respective top and side views. The blue, gray, brown, and green balls represent the Cu, N, Fe, and Se atoms, respectively.

checked the thickness of the Cu_3N slab in our calculations and found that a 10-layer slab with the bottom seven layers fixed at their bulk positions is able to simulate the insulating $\text{Cu}_3\text{N}(001)$ substrate [41]. As the in-plane lattice constant of Cu_3N ($a = b = 3.82 \text{ \AA}$) [24] is only 1.46% larger than that of FeSe (3.765 \AA) [45], we deduced that a well-defined interface can be formed in the FeSe/ Cu_3N heterostructure.

In view of the in-plane C_4 symmetry of FeSe, we studied four possible epitaxial structures for the FeSe monolayer on $\text{Cu}_3\text{N}(001)$. In Fig. 1(a), the Fe atoms sit above the N atoms and the hollow sites of the $\text{Cu}_2\text{N}(001)$ surface. The structures in Figs. 1(b) and 1(d) are constructed by shifting the FeSe monolayer in Fig. 1(a) by a quarter of a cell along the a - b direction and the a axis, respectively. In Fig. 1(c), the bottom Se atoms locate at the hollow sites of the $\text{Cu}_2\text{N}(001)$

TABLE I. Relative energies (in units of meV/Fe) of the typical AFM states (stripe, dimer, Néel) for four epitaxial structures of FeSe/ $\text{Cu}_3\text{N}(001)$ in Fig. 1 with respect to the NM state of the epitaxial structure in Fig. 1(c). After optimization, the initial structures of Figs. 1(b) and 1(d) relax to the ones similar to Figs. 1(c) and 1(a), respectively.

State	Fig. 1(a)	Fig. 1(b)	Fig. 1(c)	Fig. 1(d)
NM	17.0	1.9	0.0	17.2
Stripe	-87.9	-94.2	-95.4	-88.5
Dimer	-86.2	-94.2	-96.5	-88.5
Néel	-38.6	-48.2	-50.6	-39.4

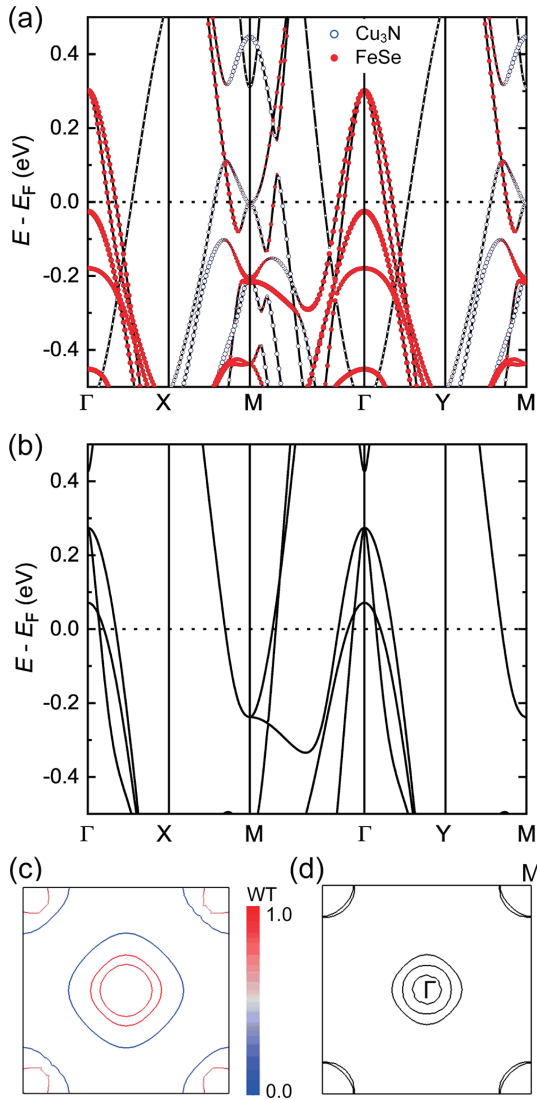


FIG. 2. Band structures of (a) FeSe/Cu₃N(001) and (b) the freestanding FeSe monolayer in the nonmagnetic states. The red dots and blue circles in (a) represent the projected bands of FeSe and Cu₃N, respectively. (c) and (d) The 2D slices of the Fermi surfaces of FeSe/Cu₃N(001) and freestanding FeSe monolayer in the nonmagnetic states, respectively. The color bar in (c) denotes the weight (WT) of the contributions from the FeSe layer.

surface. We first optimized these heterostructures without the spin polarization, i.e., in the nonmagnetic (NM) state of FeSe monolayer. By comparing their relative energies as listed in Table I, we found that the most stable structure is as depicted in Fig. 1(c), which is energetically 17.0 meV/Fe lower than the structures in Fig. 1(a). Moreover, the initial structures in Figs. 1(b) and 1(d) relax to ones similar to Figs. 1(c) and 1(a), respectively, indicating the instability of the former two structures. In the most stable structure in Fig. 1(c), the vertical distance between the lower Se layer and the Cu₂N surface is as large as 2.70 Å, which suggests a relatively weak interaction between them.

Figures 2(a) and 2(b) show the nonmagnetic band structures of monolayer FeSe on Cu₃N(001) in the epitaxy structure in Fig. 1(c) and of a freestanding FeSe mono-

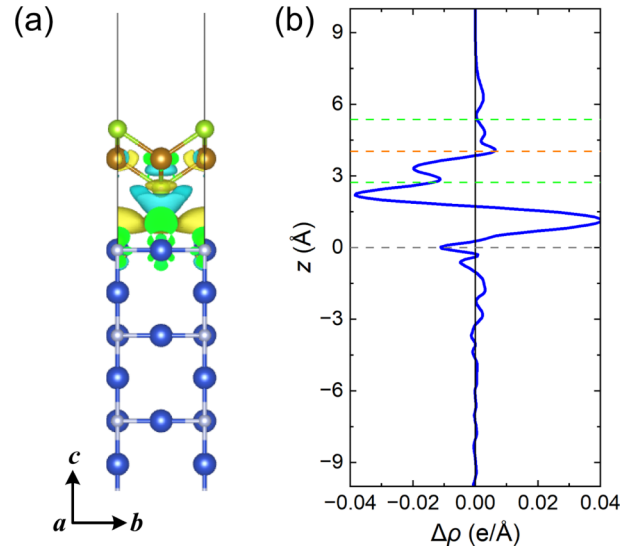


FIG. 3. (a) Three-dimensional and (b) one-dimensional differential charge densities for monolayer FeSe on Cu₃N(001) in the nonmagnetic state. The yellow and blue isosurfaces in (a), whose values are set to $3.4 \times 10^{-4} e/\text{Å}^3$, represent the electron accumulation and depletion areas, respectively. The dashed color lines in (b) mark the respective atomic positions of the Se, Fe, Se, and Cu₂N planes, while $z = 0$ presents the position of the Cu₃N(001) surface.

layer, respectively. For the freestanding FeSe monolayer, there are three hole-type pockets around the Γ point and two electron-type pockets around the M point [Fig. 2(b)], which is consistent with previous studies [46]. When the monolayer FeSe is epitaxially grown on Cu₃N(001), some obvious changes take place. In Fig. 2(a), the red dots and blue circles label the respective contributions from the FeSe monolayer and the Cu₃N substrate. Compared with the band structure of the freestanding FeSe monolayer [Fig. 2(b)], the Fermi level of FeSe/Cu₃N(001) shifts down, resulting in two enlarged hole pockets around the Γ point and two shrunken electron pockets around the M point. Correspondingly, we also exhibit the two-dimensional (2D) slices of the Fermi surfaces in Figs. 2(c) and 2(d). In Fig. 2(c), the FeSe layer in FeSe/Cu₃N mainly contributes two hole-type pockets around the Γ point and one electron-type pocket at the M point, where the volume of the former pockets is larger than that of the latter pocket. This feature indicates that there is hole doping from the Cu₃N substrate to the epitaxial FeSe monolayer.

In order to quantitatively analyze the charge transfer, we calculated the differential charge densities of FeSe/Cu₃N(001), as shown in Fig. 3. After integrating the one-dimensional charge densities from the neutral plane of the interface, i.e., the zero-charge-transfer position between the Cu₃N surface and FeSe layer, to the vacuum region, we found that there is about 0.019 hole per Fe atom doped into the epitaxial FeSe layer. In comparison, angle-resolved photoemission spectroscopy experiments suggest that in the FeSe/STO system the substrate can dope about 0.12 electron per Fe atom to the FeSe monolayer [10], which is 6 times larger in intensity than the hole-doped case here. The transferred charges in FeSe/Cu₃N(001) are also smaller than that of the (Se/S)_x(NH₃)₃Fe₂Se₂ crystal, in which there is about

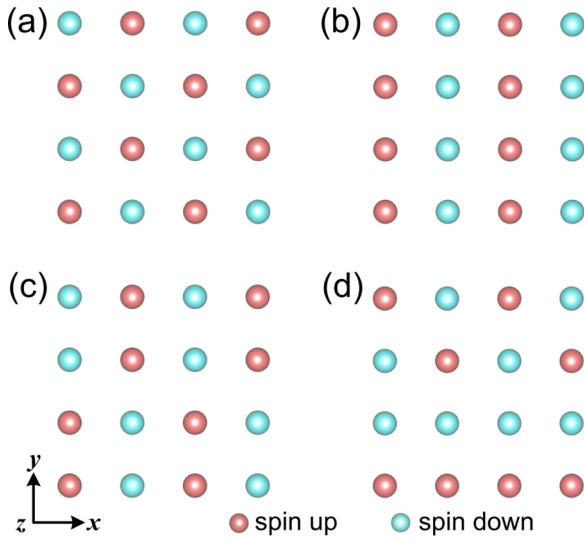


FIG. 4. Four typical spin configurations of Fe atoms in the FeSe monolayer: (a) checkerboard AFM Néel state, (b) stripe (collinear) AFM state, (c) dimer AFM state, and (d) a mixed AFM state (combined Néel and stripe AFM pattern). The x and y axes are along the $a + b$ and $-a + b$ directions, which are rotated by 45° with respect to the axes in Fig. 1. The peach and cyan balls represent the spin-up and spin-down Fe atoms, respectively.

0.14 hole per Fe atom [1]. We note that in our calculations above, we used a perfect Cu_3N substrate without defects or dopants. However, in real FeSe/ SrTiO_3 systems, either Nb dopants or O vacancies in the SrTiO_3 substrate may introduce extra electrons [12,47]. Thus, to improve the hole doping level in FeSe/ $\text{Cu}_3\text{N}(001)$, we adopted two approaches: applying electric field and introducing Cu vacancies in Cu_3N . We found that with an electric field applied vertical to the interface up to 0.3 V/\AA , the hole doping to FeSe layer slightly increases to 0.022 hole per Fe atom. In addition, the $\sqrt{2} \times 2\sqrt{2}$ slab with one Cu vacancy in the surface Cu_2N layer can dope 0.020 hole/Fe to the FeSe epitaxial layer. And when this slab with the Cu defect is under an electric field of 0.1 V/\AA , the doping level can be further improved to 0.023 hole/Fe, indicating their synergetic effect.

Since there are non-negligible spin excitations in the FeSe/STO system [11,48,49], we then studied the magnetic properties of FeSe/ $\text{Cu}_3\text{N}(001)$. Three typical AFM states for the FeSe monolayer on $\text{Cu}_3\text{N}(100)$ surface are considered (Fig. 4), including the Néel AFM, stripe AFM, and dimer AFM states. The relative energies of the magnetic configurations of four epitaxial structures after optimization are summarized in Table I. For each epitaxial structure, the dimer AFM state and the stripe AFM state have almost degenerate lowest energies, with the energy difference being smaller than 1.7 meV/Fe . This implies that magnetic frustration may exist in FeSe/ $\text{Cu}_3\text{N}(001)$, which can induce spin fluctuations and may lead to the emergence of superconductivity [11,48,50].

We also examined the electronic structure and the charge transfer effects in these AFM states, which turn out to be consistent with the NM picture, that is, about 0.017 hole/Fe doped into the epitaxial FeSe monolayer in the dimer AFM state [Fig. 5(c)] and about 0.019 hole/Fe in the stripe AFM

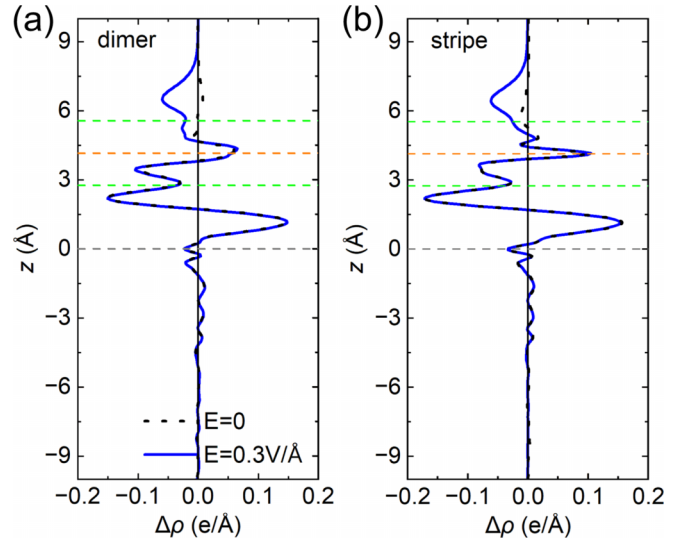


FIG. 5. One-dimensional differential charge densities for the (a) dimer and (b) stripe AFM states of monolayer FeSe on $\text{Cu}_3\text{N}(001)$. The orange, green, and gray dashed lines mark the atomic positions of the Fe, Se, and Cu_2N planes, respectively, while $z = 0$ represents the position of the $\text{Cu}_3\text{N}(001)$ surface. The blue solid lines and black dashed lines show data under an electric field of 0.3 V/\AA and no electric field, respectively.

state [Fig. 5(b)]. We further checked the effect of electric field on the charge transfer at the FeSe/ Cu_3N interface in the dimer and stripe AFM states. As shown in Fig. 5, an electric field with a strength of 0.3 V/\AA yields a doping of 0.029 (0.031) hole per Fe atom in FeSe in the dimer (stripe) AFM state. When it comes to experiments, the electric field may trigger higher doping concentrations of holes at the interface with the aid of Cu vacancies in the Cu_3N substrate [26].

In iron-based superconductors, Fe $3d$ orbitals, especially the d_{xy} , d_{xz} , and d_{yz} orbitals near the Fermi level, play important roles in the spin density wave and the superconductivity, as reported in previous experimental [51–53] and theoretical [54,55] studies. Therefore, we calculated the partial density of states (PDOS) and show the d_{xy} , d_{xz} , and d_{yz} orbitals of FeSe/ $\text{Cu}_3\text{N}(001)$ in Fig. 6. We focused on the dimer and stripe AFM states to figure out the evolution of electronic structures of FeSe before and after the epitaxial growth. First, compared with the freestanding FeSe monolayer (depicted by the dashed lines in Fig. 6), the substrate Cu_3N transfers holes into the epitaxial FeSe monolayer (solid lines in Fig. 6) and shifts the Fermi level E_F to lower energies. The variation of the Fe d_{z^2} orbital after epitaxy growth is more obvious, contributing a major DOS near E_F (not shown). Second, the splitting between the d_{xz} and d_{yz} orbitals is apparently increased in FeSe/ Cu_3N compared with the freestanding case. In addition, the DOS of the d_{xy} orbital is slightly increased in FeSe/ Cu_3N . According to previous studies [51], the inequivalent hybridization between the d_{xy} orbital and the d_{xz} or d_{yz} orbital due to the distorted Se-Fe-Se bond angle might also influence the nematicity and hence the superconductivity [56]. Last, referring to the DFT calculations [57], the d_{xy} orbital is closely aligned along the Fe-anion directions, which is more localized, introducing a larger local moment, and

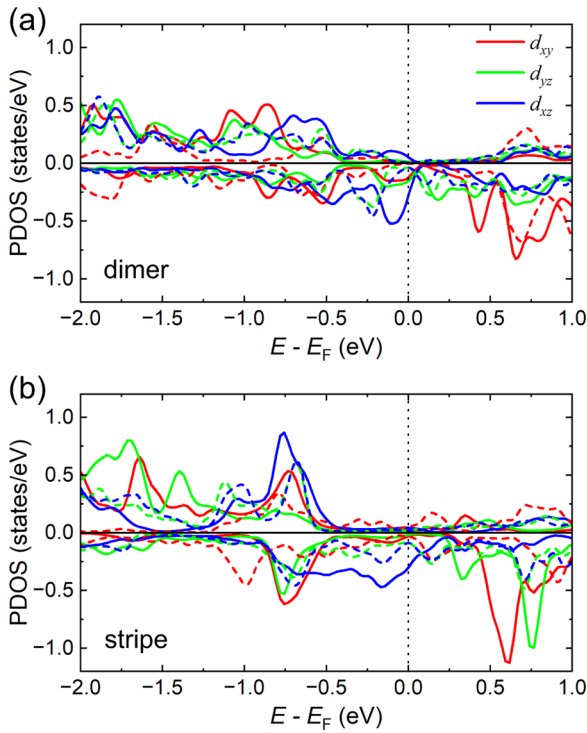


FIG. 6. Partial density of states (PDOS) of Fe d_{xy} (red), d_{xz} (blue), and d_{yz} (green) orbitals of monolayer FeSe in the (a) dimer and (b) stripe AFM states. The solid lines are data from FeSe/Cu₃N, while the dashed lines represent those of the freestanding FeSe monolayer.

more correlated due to the kinetic frustration in iron-based superconductors [57,58]. In this way, Cu₃N slightly raises the local moment of Fe in FeSe/Cu₃N and might push FeSe with a stronger correlation strength. In short, the Cu₃N substrate not only introduces the charge transfer at the interface but also is responsible for the evolution of $3d$ orbitals in FeSe.

To analyze the multiple influences introduced by the substrate in FeSe/Cu₃N(001), we sequentially applied the effects of lattice strain, asymmetric Se height, and charge doping to monolayer FeSe. First, when the in-plane lattice constant of monolayer FeSe is fixed to that of Cu₃N, the energy difference between the stripe and dimer AFM states ($\Delta E_{\text{str-dim}} = E_{\text{stripe}} - E_{\text{dimer}}$) is noticeably reduced. For the freestanding FeSe monolayer, the calculated lattice constant is about 3.68 Å, and $\Delta E_{\text{str-dim}}$ is about 15.28 meV/Fe. Once the in-plane lattice constant of the FeSe monolayer is enlarged to 3.82 Å as in Cu₃N(001), $\Delta E_{\text{str-dim}}$ is only 6.31 meV per Fe atom. This suggests that with the increasing of the in-plane lattice constant, the magnetic ground state of monolayer FeSe tends to transit from the dimer AFM state to the stripe AFM state [19], which is consistent with a previous calculation [59]. Then we fixed the in-plane lattice constant as $a_{\text{Cu}_3\text{N}}$ and compared the structure of fully optimized Se sites in a freestanding FeSe monolayer with the one in which the Se heights are obtained from FeSe/Cu₃N(001). In the latter, the upper-layer and lower-layer Se atoms differ in height from the Fe-Fe plane. It has been found that with asymmetric Se heights, $\Delta E_{\text{str-dim}}$ further decreases to 4.92 meV/Fe, suggesting that the interface-induced asymmetric Se heights also have a finite

impact on the magnetic frustration in FeSe. Finally, we fixed the structure from the last step and introduced hole doping to the isolated FeSe layer. When we doped 0.013 hole per Fe, $\Delta E_{\text{str-dim}}$ reduced to 3.97 meV/Fe. So far, $\Delta E_{\text{str-dim}}$ of monolayer FeSe under the separate effects derived from the lattice strain, asymmetric Se heights, and hole doping are still about 4 times larger than the value of FeSe on Cu₃N(001), which is only 1.06 meV/Fe, as shown in Table I. On the one hand, the Cu₃N(001) substrate has richer interfacial effects on the epitaxial FeSe monolayer, such as the electric field due to the charge redistribution at the interface and the real atomic interaction. On the other hand, all effects discussed above are static influences, while in real materials more complicated factors are involved. For instance, the interfacial phonons could also play important roles in the electronic and magnetic properties of the epitaxial FeSe monolayer [60–62]. Finally, FeSe/Cu₃N(001) is a promising playground for investigating interfacial physics.

IV. DISCUSSION AND SUMMARY

The magnetic coupling between Fe spins in the FeSe monolayer on Cu₃N(001) can be described with an effective Heisenberg model [63–65],

$$H = J_1 \sum_{\langle i,j \rangle} \mathbf{S}_i \cdot \mathbf{S}_j + J_2 \sum_{\langle\langle i,j \rangle\rangle} \mathbf{S}_i \cdot \mathbf{S}_j + J_3 \sum_{\langle\langle\langle i,j \rangle\rangle\rangle} \mathbf{S}_i \cdot \mathbf{S}_j, \quad (1)$$

where J_1 , J_2 , and J_3 respectively represent the nearest-neighbor, next-nearest-neighbor, and third-nearest-neighbor Fe-Fe spin exchanges and \mathbf{S} is the local moment of the Fe atom. From our calculated energies in the Fig. 1(c) column in Table I and the relative energy (35.6 meV/Fe) of a mixed AFM state (combined Néel and stripe AFM) [Fig. 4(d)], we obtain $J_1 = 49.1$ meV/S², $J_2 = 30.1$ meV/S², and $J_3 = 5.9$ meV/S². These exchange interactions J_i in FeSe obey the relation $J_1 \approx 2J_2 - 2J_3$, leading to the energy degeneracy of the stripe and dimer AFM states, which is similar to the degenerate case of the dimer and trimer AFM states in bulk FeSe [65].

According to previous studies [49], the magnetic fluctuation in FeSe on SrTiO₃ may contribute to the enhanced superconductivity [11]. From our calculations, the FeSe/Cu₃N(001) interface tends to induce magnetic frustration in the epitaxial FeSe monolayer as well, which might induce the interfacial superconductivity and calls for future experimental verification. While previous studies on interfacial superconductivity of monolayer FeSe concentrated on the electron doping side, the Cu₃N substrate proposed here provides the complementary hole doping side. Similar to previous works on hole-doped and electron-doped cuprate superconductors [66–69] and FeAs-based superconductors [70–73], our studies may help provide a comprehensive view of the unconventional superconductivity in FeSe-based compounds.

As to the doping from substrates to monolayer FeSe, many reports have indicated that FeSe-based interfacial systems typically exhibit higher electron doping levels; for example, the SrTiO₃ substrate dopes about 0.12 electron per Fe to the FeSe layer [10]. In this work, we attribute the difficulty in the enhancement of hole doping in FeSe to the modest variation of the work function of the Cu₃N substrate after modulation.

From our calculations, the work function of monolayer FeSe with the in-plane lattice constant of Cu_3N is 4.55 eV, while the work function of undoped Cu_3N is 5.12 eV, resulting in the hole transfer from Cu_3N into FeSe. Previous studies showed that Cu_3N is a bipolar semiconductor, which could be p type doped by interstitial F atoms [74] (or Cu vacancies [26]) and n type doped by substituting N with O atoms [75]. However, the calculated work functions of Cu_3N substrates with 5% F and 5% O dopings are 5.10 and 4.85 eV, respectively, which are still higher than that of FeSe, and both lead to the hole doping. As for the work function of a Cu_3N substrate with 1.7% Cu vacancies, it is 5.14 eV, which is similar to the undoped and F-doped cases. The interfacial charge transfer in FeSe on doped Cu_3N is around 0.02 hole/Fe, consistent with the above variations in the work functions of Cu_3N . It is thus advisable to search for a lattice-matched substrate with a higher work function and shallow p -type dopants to further explore the superconductivity in hole-doped FeSe.

In conclusion, we have systematically studied the electronic and magnetic properties of the FeSe monolayer on a $\text{Cu}_3\text{N}(001)$ substrate through first-principles calculations. We found that the preferential epitaxial position for the monolayer FeSe on $\text{Cu}_3\text{N}(001)$ is for the bottom-layer Se atoms of FeSe to locate above the hollow sites of the Cu_2N surface layer. According to our calculations, the dimer AFM

state and the stripe AFM state of FeSe on $\text{Cu}_3\text{N}(001)$ are almost energetically degenerated, resulting from synergistic effects such as the in-plane lattice strain, unsymmetrical Se heights, and charge redistributions due to the Cu_3N substrate. Furthermore, the Cu_3N substrate naturally dopes holes into the FeSe monolayer, while the electric field and/or the Cu vacancies in Cu_3N could partially tune the hole doping level. Combined with the magnetic frustration in FeSe, this indicates the possibility of emergent unconventional superconductivity in FeSe/ $\text{Cu}_3\text{N}(001)$. Herein, our results provide an interesting platform to study the potential hole-doped superconductivity in the FeSe interfacial system, which could offer good contrast with the electron doping case.

ACKNOWLEDGMENTS

We wish to thank S. Gao for stimulating discussions. This work was supported by the National Key R&D Program of China (Grants No. 2022YFA1403103 and No. 2019YFA0308603), the National Natural Science Foundation of China (Grants No. 12174443 and No. 11934020), and the Beijing Natural Science Foundation (Grant No. Z200005). Computational resources were provided by the Physical Laboratory of High Performance Computing at Renmin University of China and the Beijing Super Cloud Computing Center.

-
- [1] R. Sun, S. Jin, L. Gu, Q. Zhang, Q. Huang, T. Ying, Y. Peng, J. Deng, Z. Yin, and X. Chen, *J. Am. Chem. Soc.* **141**, 13849 (2019).
- [2] X. Dong, H. Zhou, H. Yang, J. Yuan, K. Jin, F. Zhou, D. Yuan, L. Wei, J. Li, X. Wang, G. Zhang, and Z. Zhao, *J. Am. Chem. Soc.* **137**, 66 (2015).
- [3] Q. Ma, F. Lan, W. Qiu, X. Li, Z. Ma, H. Li, and Y. Liu, *J. Mater. Chem. C* **7**, 10019 (2019).
- [4] J. P. Sun, K. Matsuura, G. Z. Ye, Y. Mizukami, M. Shimozaawa, K. Matsubayashi, M. Yamashita, T. Watashige, S. Kasahara, Y. Matsude, J.-Q. Yan, B. C. Sales, Y. Uwatoko, J.-G. Cheng, and T. Shibauchi, *Nat. Commun.* **7**, 12146 (2016).
- [5] B. Lei, J. H. Cui, Z. J. Xiang, C. Shang, N. Z. Wang, G. J. Ye, X. G. Luo, T. Wu, Z. Sun, and X. H. Chen, *Phys. Rev. Lett.* **116**, 077002 (2016).
- [6] F.-C. Hsu, J.-Y. Luo, K.-W. Yeh, T.-K. Chen, T.-W. Huang, P. M. Wu, Y.-C. Lee, Y.-L. Huang, Y.-Y. Chu, D.-C. Yan, and M.-K. Wu, *Proc. Natl. Acad. Sci. USA* **105**, 14262 (2008).
- [7] J. Guo, S. Jin, G. Wang, S. Wang, K. Zhu, T. Zhou, M. He, and X. Chen, *Phys. Rev. B* **82**, 180520(R) (2010).
- [8] B. L. Kang, M. Z. Shi, S. J. Li, H. H. Wang, Q. Zhang, D. Zhao, J. Li, D. W. Song, L. X. Zheng, L. P. Nie, T. Wu, and X. H. Chen, *Phys. Rev. Lett.* **125**, 097003 (2020).
- [9] Q.-Y. Wang, Z. Li, W.-H. Zhang, Z.-C. Zhang, J.-S. Zhang, W. Li, H. Ding, Y.-B. Ou, P. Deng, K. Chang, J. Wen, C.-L. Song, K. He, J.-F. Jia, S.-H. Ji, Y.-Y. Wang, L.-L. Wang, X. Chen, X.-C. Ma, and Q.-K. Xue, *Chin. Phys. Lett.* **29**, 037402 (2012).
- [10] S. He *et al.*, *Nat. Mater.* **12**, 605 (2013).
- [11] S. Tan, Y. Zhang, M. Xia, Z. Ye, F. Chen, X. Xie, R. Peng, D. Xu, Q. Fan, H. Xu, J. Jiang, T. Zhang, X. Lai, T. Xiang, J. Hu, B. Xie, and D. Feng, *Nat. Mater.* **12**, 634 (2013).
- [12] J.-F. Ge, Z.-L. Liu, C. Liu, C.-L. Gao, D. Qian, Q.-K. Xue, Y. Liu, and J.-F. Jia, *Nat. Mater.* **14**, 285 (2015).
- [13] D. F. Liu, W. H. Zhang, D. X. Mou, J. F. He, Y.-B. Ou, Q.-Y. Wang, Z. Li, L. L. Wang, L. Zhao, S. L. He *et al.*, *Nat. Commun.* **3**, 931 (2012).
- [14] W. Zhao, M. Li, C.-Z. Chang, J. Jiang, L. Wu, C. Liu, J. S. Moodera, Y. Zhu, and M. H. W. Chan, *Sci. Adv.* **4**, eaao2682 (2018).
- [15] J. J. Lee, F. T. Schmitt, R. G. Moore, S. Johnston, Y.-T. Cui, W. Li, M. Yi, Z. K. Liu, M. Hashimoto, Y. Zhang, D. H. Lu, T. P. Devereaux, D.-H. Lee, and Z.-X. Shen, *Nature (London)* **515**, 245 (2014).
- [16] R. Peng, H. C. Xu, S. Y. Tan, H. Y. Cao, M. Xia, X. P. Shen, Z. C. Huang, C. H. P. Wen, Q. Song, T. Zhang, B. P. Xie, X. G. Gong, and D. L. Feng, *Nat. Commun.* **5**, 5044 (2014).
- [17] S. Zhang, T. Wei, J. Guan, Q. Zhu, W. Qin, W. Wang, J. Zhang, E. W. Plummer, X. Zhu, Z. Zhang, and J. Guo, *Phys. Rev. Lett.* **122**, 066802 (2019).
- [18] K. Liu, Z.-Y. Lu, and T. Xiang, *Phys. Rev. B* **85**, 235123 (2012).
- [19] K. Liu, M. Gao, Z.-Y. Lu, and T. Xiang, *Chin. Phys. B* **24**, 117402 (2015).
- [20] H. Ding, Y.-F. Lv, K. Zhao, W.-L. Wang, L. Wang, C.-L. Song, X. Chen, X.-C. Ma, and Q.-K. Xue, *Phys. Rev. Lett.* **117**, 067001 (2016).
- [21] S. N. Rebec, T. Jia, C. Zhang, M. Hashimoto, D.-H. Lu, R. G. Moore, and Z.-X. Shen, *Phys. Rev. Lett.* **118**, 067002 (2017).
- [22] G. Zhou, Q. Zhang, F. Zheng, D. Zhang, C. Liu, X. Wang, C.-L. Song, K. He, X.-C. Ma, L. Gu, P. Zhang, L. Wang, and Q.-K. Xue, *Sci. Bull.* **63**, 747 (2018).

- [23] Y. Song, Z. Chen, Q. Zhang, H. Xu, X. Lou, X. Chen, X. Xue, X. Zhu, R. Tao, T. Yu, H. Ru, Y. Wang, T. Zhang, J. Guo, L. Gu, Y. Xie, R. Peng, and D. Feng, *Nat. Commun.* **12**, 5926 (2021).
- [24] D. M. Borsa and D. O. Boerma, *Surf. Sci.* **548**, 95 (2004).
- [25] K. J. Kim, J. H. Kim, and J. H. Kang, *J. Cryst. Growth* **222**, 767 (2001).
- [26] A. N. Fioretti, C. P. Schwartz, J. Vinson, D. Nordlund, D. Prendergast, A. C. Tamboli, C. M. Caskey, F. Tuomisto, F. Linez, S. T. Christensen, E. S. Toberer, S. Lany, and A. Zakutayev, *J. Appl. Phys.* **119**, 181508 (2016).
- [27] C. Navío, M. J. Capitán, J. Álvarez, F. Yndurain, and R. Miranda, *Phys. Rev. B* **76**, 085105 (2007).
- [28] P. Hohenberg and W. Kohn, *Phys. Rev.* **136**, B864 (1964).
- [29] W. Kohn and L. J. Sham, *Phys. Rev.* **140**, A1133 (1965).
- [30] P. E. Blöchl, *Phys. Rev. B* **50**, 17953 (1994).
- [31] G. Kresse and D. Joubert, *Phys. Rev. B* **59**, 1758 (1999).
- [32] G. Kresse and J. Furthmüller, *Phys. Rev. B* **54**, 11169 (1996).
- [33] J. P. Perdew, K. Burke, and M. Ernzerhof, *Phys. Rev. Lett.* **77**, 3865 (1996).
- [34] S. Grimme, *J. Comput. Chem.* **27**, 1787 (2006).
- [35] X. Wu, M. C. Vargas, S. Nayak, V. Lotrich, and G. Scoles, *J. Chem. Phys.* **115**, 8748 (2001).
- [36] H. J. Monkhorst and J. D. Pack, *Phys. Rev. B* **13**, 5188 (1976).
- [37] V. Wang, N. Xu, J.-C. Liu, G. Tang, and W. Geng, *Comput. Phys. Commun.* **267**, 108033 (2021).
- [38] M. Kawamura, *Comput. Phys. Commun.* **239**, 197 (2019).
- [39] S. L. Dudarev, G. A. Botton, S. Y. Savrasov, C. J. Humphreys, and A. P. Sutton, *Phys. Rev. B* **57**, 1505 (1998).
- [40] A. Ferrón, J. L. Lado, and J. Fernández-Rossier, *Phys. Rev. B* **92**, 174407 (2015).
- [41] M. J. Winiarski, *J. Solid State Chem.* **266**, 161 (2018).
- [42] A. Jiang, M. Qi, and J. Xiao, *J. Mater. Sci. Technol.* **34**, 1467 (2018).
- [43] F. Zheng, F. Wang, Z. Kang, and P. Zhang, *Sci. Rep.* **3**, 2213 (2013).
- [44] H. T. Ali, Z. Tanveer, M. R. Javed, K. Mahmood, N. Amin, S. Ikram, A. Ali, M. R. H. Shah Gilani, M. A. Sajjad, and M. Yusuf, *Optik* **245**, 167666 (2021).
- [45] D. Louca, K. Horigane, A. Llobet, R. Arita, S. Ji, N. Katayama, S. Konbu, K. Nakamura, T.-Y. Koo, P. Tong, and K. Yamada, *Phys. Rev. B* **81**, 134524 (2010).
- [46] T. Bazhiron and M. L. Cohen, *J. Phys.: Condens. Matter* **25**, 105506 (2013).
- [47] K. V. Shanavas and D. J. Singh, *Phys. Rev. B* **92**, 035144 (2015).
- [48] Y. Zhou, L. Miao, P. Wang, F. F. Zhu, W. X. Jiang, S. W. Jiang, Y. Zhang, B. Lei, X. H. Chen, H. F. Ding, H. Zheng, W. T. Zhang, J.-F. Jia, D. Qian, and D. Wu, *Phys. Rev. Lett.* **120**, 097001 (2018).
- [49] Q. Wang, W. Zhang, W. Chen, Y. Xing, Y. Sun, Z. Wang, J.-W. Mei, Z. Wang, L. Wang, X.-C. Ma, F. Liu, Q.-K. Xue, and J. Wang, *2D Mater.* **4**, 034004 (2017).
- [50] C. Liu, Z. Wang, Y. Gao, X. Liu, Y. Liu, Q.-H. Wang, and J. Wang, *Phys. Rev. Lett.* **123**, 036801 (2019).
- [51] M. Yi, Y. Zhang, Z.-X. Shen, and D. Lu, *npj Quantum Mater.* **2**, 57 (2017).
- [52] A. Kostin, P. O. Sprau, A. Kreisel, Y. X. Chong, A. E. Bohmer, P. C. Canfield, P. J. Hirschfeld, B. M. Andersen, and J. C. Seamus Davis, *Nat. Mater.* **17**, 869 (2018).
- [53] D. Liu *et al.*, *Phys. Rev. X* **8**, 031033 (2018).
- [54] Z. Wang, P. Zhang, G. Xu, L. K. Zeng, H. Miao, X. Xu, T. Qian, H. Weng, P. Richard, A. V. Fedorov, H. Ding, X. Dai, and Z. Fang, *Phys. Rev. B* **92**, 115119 (2015).
- [55] Y. Su, H. Liao, and T. Li, *J. Phys.: Condens. Matter* **27**, 105702 (2015).
- [56] W. Li, Y. Zhang, P. Deng, Z. Xu, S.-K. Mo, M. Yi, H. Ding, M. Hashimoto, R. G. Moore, D.-H. Lu, X. Chen, Z.-X. Shen, and Q.-K. Xue, *Nat. Phys.* **13**, 957 (2017).
- [57] D. W. Tam, Z. Yin, Y. Xie, W. Wang, M. B. Stone, D. T. Adroja, H. C. Walker, M. Yi, and P. Dai, *Phys. Rev. B* **102**, 054430 (2020).
- [58] Z. P. Yin, K. Haule, and G. Kotliar, *Nat. Mater.* **10**, 932 (2011).
- [59] H.-Y. Cao, S. Chen, H. Xiang, and X.-G. Gong, *Phys. Rev. B* **91**, 020504(R) (2015).
- [60] Q.-Q. Ye, K. Liu, and Z.-Y. Lu, *Phys. Rev. B* **88**, 205130 (2013).
- [61] K. Liu, B.-J. Zhang, and Z.-Y. Lu, *Phys. Rev. B* **91**, 045107 (2015).
- [62] T. Li, X. Zhang, and Z. Zeng, *Phys. Chem. Chem. Phys.* **23**, 25107 (2021).
- [63] F. Ma, Z.-Y. Lu, and T. Xiang, *Phys. Rev. B* **78**, 224517 (2008).
- [64] F. Ma, W. Ji, J. Hu, Z.-Y. Lu, and T. Xiang, *Phys. Rev. Lett.* **102**, 177003 (2009).
- [65] K. Liu, Z.-Y. Lu, and T. Xiang, *Phys. Rev. B* **93**, 205154 (2016).
- [66] Y. Krockenberger, J. Kurian, A. Winkler, A. Tsukada, M. Naito, and L. Alff, *Phys. Rev. B* **77**, 060505(R) (2008).
- [67] M. Horio and A. Fujimori, *J. Phys.: Condens. Matter* **30**, 503001 (2018).
- [68] R. L. Greene, P. R. Mandal, N. R. Poniatowski, and T. Sarkar, *Annu. Rev. Condens. Matter Phys.* **11**, 213 (2020).
- [69] C. Lin, T. Adachi, M. Horio, T. Ohgi, M. A. Baqiya, T. Kawamata, H. Sato, T. Sumura, K. Koshiishi, S. Nakata, G. Shibata, K. Hagiwara, M. Suzuki, K. Ono, K. Horiba, H. Kumigashira, S. Ideta, K. Tanaka, Y. Koike, and A. Fujimori, *Phys. Rev. Res.* **3**, 013180 (2021).
- [70] M. Rotter, M. Tegel, and D. Johrendt, *Phys. Rev. Lett.* **101**, 107006 (2008).
- [71] M. Rotter, M. Pangerl, M. Tegel, and D. Johrendt, *Angew. Chem. Int. Ed.* **47**, 7949 (2008).
- [72] A. S. Sefat, R. Jin, M. A. McGuire, B. C. Sales, D. J. Singh, and D. Mandrus, *Phys. Rev. Lett.* **101**, 117004 (2008).
- [73] J.-H. Chu, J. G. Analytis, C. Kucharczyk, and I. R. Fisher, *Phys. Rev. B* **79**, 014506 (2009).
- [74] K. Matsuzaki, K. Harada, Y. Kumagai, S. Koshiya, K. Kimoto, S. Ueda, M. Sasase, A. Maeda, T. Susaki, M. Kitano, F. Oba, and H. Hoson, *Adv. Mater.* **30**, 1801968 (2018).
- [75] M. Zervos, A. Othonos, T. Pavloudis, S. Giaremis, J. Kioseoglou, K. Mavridou, M. Katsikini, F. Pinakidou, and E. C. Paloura, *J. Phys. Chem. C* **125**, 3680 (2021).